MNRAS **000**, 1–12 (2019) Preprint 5 July 2019 Compiled using MNRAS LATEX style file v3.0

Tidally Trapped Pulsations in HD 74423 discovered by TESS

G. Handler,[1⋆] J. Fuller,[2] D. W. Kurtz,[3] S. A. Rappaport,[4] H. Saio,[5]
S. Chowdhury,[1] P. Sowicka,[1] R. Gagliano,[6] T. L. Jacobs,[7] A. Vanderburg[8,9]
[1]*Nicolaus Copernicus Astronomical Center, Polish Academy of Sciences, ul. Bartycka 18, 00-716, Warszawa, Poland*
[2]*Division of Physics, Mathematics and Astronomy, California Institute of Technology, Pasadena, CA 91125, USA*
[3]*Jeremiah Horrocks Institute, University of Central Lancashire, Preston PR1 2HE, UK*
[4]*Department of Physics, and Kavli Institute for Astrophysics and Space Research, M.I.T., Cambridge, MA 02139, USA*
[5]*Astronomical Institute, Graduate School of Science, Tohoku University, Sendai 980-8578, Japan*
[6]*Planet Hunters*
[7]*Amateur Astronomer, 12812 SE 69th Place Bellevue, WA 98006*
[8]*Department of Astronomy, The University of Texas at Austin, 2515 Speedway, Stop C1400, Austin, TX 78712*
[9]*NASA Sagan Fellow*

Accepted XXX. Received YYY; in original form ZZZ

ABSTRACT
We report the discovery of tidally trapped pulsations in the ellipsoidal variable HD 74423, containing a δ Scuti pulsator in a 1.6-d orbit with a low-mass companion star. The pulsating primary star is nearly filling its Roche lobe, and the pulsations have much larger amplitude in the hemisphere that faces the currently undetected secondary star. We interpret this as an obliquely pulsating distorted dipole oscillation with a pulsation axis aligned with the tidal axis. This is the first time such a phenomenon has been observed. We present a simple physical model demonstrating how stellar oscillations can be tidally trapped and amplified near the star's L1 point.

Key words: keyword1 – keyword2 – keyword3

1 INTRODUCTION

Much of the present-day understanding of the universe is rooted in the knowledge of the basic parameters and structure of the stars. Their precise determinations rest on two methods: the analysis of eclipsing binary stars and asteroseismology. Whereas detached eclipsing binaries facilitate the determination of global stellar parameters to the highest precision (e.g. see Torres, Andersen & Giménez 2010), asteroseismology allows the determination of interior stellar structure to fine detail (Aerts, Christensen-Dalsgaard & Kurtz 2010). Even more rewarding would then be asteroseismic analyses of the components of detached eclipsing binaries. However, such objects are rare.

Proximity effects between binary star components can influence stellar oscillations. The modification of interior stellar structure due to mass transfer could be traced asteroseismically. Many decades ago it has been theoretically predicted that the excitation of stellar oscillations can be augmented by tides (Cowling 1941), but convincing observational evidence was accumulated only in the more recent past (Handler et al. 2002).

⋆ E-mail: gerald@camk.edu.pl

It was only with the advent of the *Kepler* space telescope that binary components whose oscillations were affected by tides were discovered in larger numbers. Most prominent among them are the highly eccentric binary "Heartbeat" stars (e.g., Welsh et al. 2011; Thompson et al. 2012; Hambleton et al. 2013, 2018). These stars show overtone pressure modes that are exactly resonant with high harmonics of the orbital frequency.

Aside from that, it has been speculated (Balona 1985) that a binary companion could cause precession of the stellar pulsation axis, which would result in amplitude modulation of a nonradial pulsation over the orbit. This, of course, is no different from what had already been observed in the rapidly oscillating Ap (roAp) stars (Kurtz 1982). In the latter case, however, it is the magnetic field of these stars that tilts the pulsation axis.

The roAp stars show high radial overtone, nonradial pulsation modes with frequency multiplets that have frequency separations close to the known rotation frequency for a particular Ap star, which is determined with precision from rotational variations caused by long-term abundance spots. In the asymptotic regime, Ledoux (1951) showed that

when $n >> \ell$, where n is the radial overtone and ℓ is the degree of a p mode,

$$\omega_{\ell,m} = \omega_{\ell,0} + \mathrm{m}(1 - C_{n,\ell})\Omega, \quad (1)$$

where ω is the pulsation frequency, Ω is the rotation frequency and $C_{n,\ell}$ is the 'Ledoux constant', which for p modes usually differs from zero by only a few per cent. Kurtz (1982) was able to show for the roAp stars that $C_{n,\ell}$ is zero, if equation 1 is applied, and he proposed instead the oblique pulsator model, where the pulsation axis is the magnetic axis, which is known to be oblique to the rotation axis in most Ap stars. The roAp stars thus became the first pulsating stars where it could be shown that the pulsation axis was *not* the rotation axis. There were many subsequent developments of the oblique pulsator model, and it is now believed that the pulsations axis is neither the magnetic axis, not the rotation axis, but rather lies along a plane between those (Bigot & Kurtz 2011).

With it being clear from the roAp stars that nonradially pulsating stars can have pulsation axes other than the rotation axis, an obvious idea is that in close binary stars, the tidal distortion may not only tilt the pulsation axis as suggested by Balona (1985), but even be sufficient to make the line of apsides the pulsation axis. Searches for this new type of obliquely pulsating stars have been ongoing with high precision Kepler mission data, and now with the new TESS data. However, no pattern of frequencies typical of oblique pulsation, as in the roAp stars, was found.

Until now.

1.1 HD 74423

HD 74423 is a $V = 8.61$ magnitude A-type star in the Southern Hemisphere. As such, there is not much information on it in the literature. Houk & Cowley (1975) gave a spectral type of A1V. Four decades later, Bernhard et al. (2015) reported photometric variability with a period of 0.79037(1) d and a peak to peak amplitude of 0.08 mag found in ASAS-3 data (Pojmański 2002). On this basis, they classified HD 74423 as a candidate photometrically variable chemically peculiar star.

It comes as a surprise in this picture that Gray et al. (2017) reported HD 74423 as a chemically peculiar star of the λ Bootis type, with a spectral type of A7V kA0mA0, and determined $T_{\rm eff} = 8100$ K, $\log g = 3.6$, $[M/H] = -1$ and $E(B-V) = 0.055$, consistent with this classification. The chemical peculiarity of λ Bootis stars is believed to stem from accretion of metal-depleted gas from either the interstellar medium or from a circumstellar disk or shell (Venn & Lambert 1990). Because searches for magnetic fields in λ Bootis stars (Bohlender & Landstreet 1990) have not yielded positive results to date, the current understanding is that, unlike the roAp stars, λ Bootis stars do not have surface spots. Therefore, the possible presence of rotational variability of this star is suspect, and we show below that HD 74423 instead exhibits binary ellipsoidal modulation.

2 OBSERVATIONS AND THEIR ANALYSIS

2.1 *TESS*

HD 74423 = TIC 355151781 was observed by *TESS* in sectors 9, 10 and 11 in 2-min cadence. The data have a time span of 79.8 d with a centre point in time of t_0 = BJD 2458583.99411, and comprise 50146 data points after a few outliers were removed after inspection by eye. This t_0 was used to begin the analysis, but later changed to the time of rotational light extremum, and to test the oblique pulsator model. For the assessment of phase errors with nonlinear least-squares fitting, it is important that the t_0 chosen is near to the centre of the data set. Since frequency and phase are degenerately coupled in the fitting of sinusoids, when t_0 is not the centre of the data set, small changes in frequency result in very large changes in phase, since phase is referenced from t_0.

The top panel of Fig. 1 shows a section of the initial light curve (the full light curve is too compressed to see the details) where the variations already reported by Bernhard et al. (2015) are obvious. However, the light curve shows minima of alternating depth whereas the maxima do not alternate. This type of light curve is characteristic for an ellipsoidal (Morris 1985) and less reminiscent of a rotational variable as implied by Bernhard et al. (2015). The differing minima arise from differential gravity darkening near the L1 and L2 points of the tidally distorted star. In the lower panel of Fig. 1, the orbital variability has been removed, which shows that the amplitude of the pulsation is clearly modulated with the orbit.

To stress the details of the orbital modulation of the pulsations, Fig. 2 shows the light curve folded over the orbit. The pulsation amplitude is clearly larger during the deeper minimum, i.e. in the hemisphere that points toward the secondary star. We therefore face the curious situation that the pulsations are apparently mostly confined to one hemisphere of the star.

The *TESS* data were analysed using a Discrete Fourier Transform (Kurtz 1985) to produce amplitude spectra. The top panel of Fig. 3 shows the initial amplitude spectrum, where the second harmonic of the orbital frequency is the highest peak, as we expect for a double-wave, ellipsoidal light curve in a close binary. The derived orbital frequency is $\nu_{\rm orb} = 0.6326218 \pm 0.0000006\,{\rm d}^{-1}$ ($P_{\rm orb} = 1.580723 \pm 0.000002$ d). This derivation is made from data with the pulsation frequencies removed, so that they do not contribute to the error calculation for the orbital frequency.

The second panel of Fig. 3 shows the amplitude spectrum of the residuals after a five-harmonic fit of the orbital variation $\nu_{\rm orb}$ has been pre-whitened from the data. The pulsation multiplet and two of its harmonics are visible in this panel, as are low frequency peaks that are instrumental artefacts. We removed those low frequency artefacts with a high-pass filter to produce the amplitude spectrum in the third panel, which shows only the pulsation frequency and its orbital sidelobes and harmonics. The purpose of removing the low frequency artefacts was to obtain better error estimates that do not contain instrumental variance.

From the third panel in Fig. 3, it is apparent that most of the pulsational variation is represented by a frequency multiplet centred on the highest peak. By extracting the frequencies in this multiplet and examining their frequency

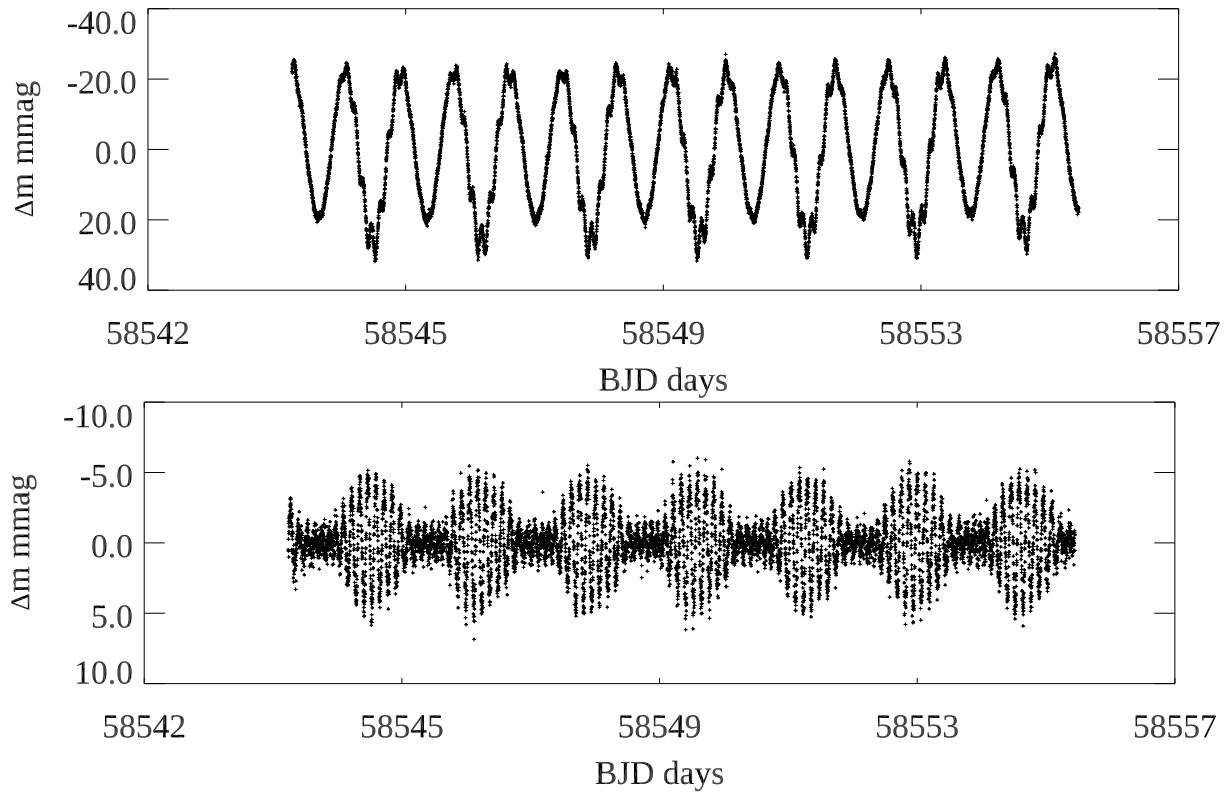

Figure 1. Top: A section of the *TESS* light curve of HD 74423 showing the clear ellipsoidal variations, along with higher frequency pulsations. The sections of the light curve not shown are similar. Bottom: The same section of the light curve after pre-whitening the orbital variations and low frequency artefacts. The modulation of the pulsation amplitude with the orbital period is striking.

separations, it is apparent that all are separated within the errors by the orbital frequency, $\nu_{\rm orb} = 0.6326218 \pm 0.0000006\,{\rm d}^{-1}$. There is, therefore, only one pulsation frequency, $\nu_1 = 8.756917 \pm 0.000010\,{\rm d}^{-1}$, and its orbital sidelobes and harmonics.[1] The harmonic multiplets are likewise separated by $\nu_{\rm orb}$. We therefore used a combination of linear and nonlinear least-squares fitting to optimise the frequencies for the multiplets. Table 1 shows the results of those procedures. The phase of the pulsation frequency and its first sidelobes are very close to equal at the time when the line of sight is along the orbital line of apsides. This is a clear signature of oblique pulsation along that axis. We note that the frequency ratio of the pulsation frequency to the orbital frequency is 13.84226 ± 0.00003, which is nearly 6000σ away from an integer, hence the pulsation is not in tidal resonance.

Finally, we fitted the pulsation frequency $\nu_1 = 8.756917\,{\rm d}^{-1}$ by least-squares to sections of the data 0.1-d long to examine the amplitude and phase variations over the orbital cycle. We also binned the original light curve by a factor of 100 – i.e., into 200-min time bins – and plot all three curves in Fig. 4. This figure shows that orbital light minimum and pulsation maximum coincide at the time when the line of sight is along the line of apsides, with the L1 point of the pulsating (primary) star facing toward us.

There is, in principle, a small contribution to the multiplet sidelobes because of the frequency variation caused by the orbital motion (Doppler shift) known as frequency modulation (FM). The relative amplitudes of the first sidelobes compared to that of the central frequency for this effect is given by equation 21 of Shibahashi & Kurtz (2012). Note, however, that there its a typographical error in that equation; the first term should be $(2\pi G)^{\frac{1}{3}}/{\rm c}$. Applying the correct form of that equation gives $\alpha \sim 0.001$. That is, the sidelobes generated by the frequency modulation are only 1/1000 the amplitude of the central peak, and this is negligible in our case here – being only half of the error in the amplitude determination – and can be ignored.

We have tried to fit the variation of the pulsation amplitude and phase over the orbit in analogy to magnetically induced variability in the roAp stars. We assume luminosity variations arise from the temperature variation δT on the stellar surface, which can be decomposed into spherical harmonics

$$\delta T \propto e^{i\omega t} \sum_{\ell=0}^{2} A_\ell Y_\ell^0(\theta_{\rm p}, \phi_{\rm p}), \qquad (2)$$

where $(\theta{\rm p}, \phi_{\rm p})$ represent spherical co-ordinates whose axis aligns with the line of apsides; i.e., we assume the pulsation is axisymmetric about the tidal axis. Converting the coordinate $(\theta_{\rm p}, \phi_{\rm p})$ to the coordinate whose axis is the rotation axis, and to the inertial coordinate whose axis is along the

[1] The amplitude of signal $\nu_1 - \nu_{\rm orb}$ is similar to that of ν_1 itself which makes it another candidate to be the real pulsation frequency. However, the presence of the second harmonic triplet that is symmetric around $3\nu_1$ clearly argues against that hypothesis.

Table 1. A least squares fit of the frequency multiplets for ν_1 and its harmonics. The zero point for the phases, $t_0 = 2458584.78684$, has been chosen to be a time when the two first orbital sidelobes have equal phase; note that those are both -1.833 rad, and the phase of ν_1 is close to these. This choice is independent of the orbital variations, but notice the orbital phase for comparison. It can be seen that orbital light minimum coincides with pulsation maximum, as expected in the oblique pulsator model.

	frequency d^{-1}	amplitude mmag ± 0.004	phase radians
$\nu_1 - 5\nu_{\rm orb}$	5.593807	0.032	-1.100 ± 0.119
$\nu_1 - 4\nu_{\rm orb}$	6.226429	0.017	1.736 ± 0.216
$\nu_1 - 3\nu_{\rm orb}$	6.859051	0.228	1.985 ± 0.017
$\nu_1 - 2\nu_{\rm orb}$	7.491673	0.292	-1.751 ± 0.013
$\nu_1 - \nu_{\rm orb}$	8.124295	1.757	-1.833 ± 0.002
ν_1	8.756917	1.894	-2.129 ± 0.002
$\nu_1 + \nu_{\rm orb}$	9.389539	0.656	-1.833 ± 0.006
$\nu_1 + 2\nu_{\rm orb}$	10.022161	0.057	1.427 ± 0.066
$\nu_1 + 3\nu_{\rm orb}$	10.654783	0.195	-1.524 ± 0.019
$\nu_1 + 4\nu_{\rm orb}$	11.287405	0.039	-1.562 ± 0.096
$\nu_1 + 5\nu_{\rm orb}$	11.920027	0.012	2.125 ± 0.309
$2\nu_1 - 2\nu_{\rm orb}$	16.248589	0.036	-0.077 ± 0.105
$2\nu_1 - \nu_{\rm orb}$	16.881211	0.090	-1.082 ± 0.042
$2\nu_1$	17.513833	0.086	2.381 ± 0.043
$2\nu_1 + \nu_{\rm orb}$	18.146455	0.157	2.467 ± 0.024
$2\nu_1 + 2\nu_{\rm orb}$	18.779077	0.060	2.555 ± 0.062
$3\nu_1 - \nu_{\rm orb}$	25.638128	0.025	-1.822 ± 0.151
$3\nu_1$	26.270750	0.053	-1.482 ± 0.071
$3\nu_1 + \nu_{\rm orb}$	26.903372	0.038	-1.638 ± 0.098

line of sight, and then integrating the visual hemisphere at each epoch, we obtain the luminosity variation as a function of time as

$$\Delta L(t) \propto \sum_{\ell=0}^{2} \sqrt{2\ell+1} A_\ell \sum_{m=-\ell}^{\ell} d^\ell_{m,0}(\beta) d^\ell_{0,m}(i_o) e^{-im\Omega t}, \qquad (3)$$

where the coefficients $d^\ell_{m,0}(\beta)$ and $d^\ell_{0,m}(i_o)$ arise in converting the coordinate $(\theta_{\rm p}, \phi_{\rm p})$ to the one associated with the rotation axis (the pulsation axis is inclined to the rotation axis by β) and to the coordinate axis associated with the line of sight (the line-of-sight is inclined to the rotation axis by angle i_o, see e.g., Saio & Gautschy 2004; Unno et al. 1989 for details).

We have assumed $\beta = 90°$ for a pulsation axis in the orbital plane, and have also assumed an inclination angle $i_o = 40°$. We then searched for a set of amplitude ratios $(A_1, A_2)/A_0$ (which are complex numbers in general) to best reproduce the observed amplitude and phase modulation of HD 74423 (Fig. 4). The best fit model obtained with $A_1/A_0 = (-1.3, -0.4)$ and $A_2/A_1 = (1.0, 0.0)$. The amplitude and phase modulations and amplitudes of side-lobes are compared with the observed ones in Fig. 5. Except at the orbital phase of 0.3 and 0.7, the phase and amplitude variabilities are reasonably reproduced, showing the pulsation is largely confined to the hemisphere toward the companion. The deviations between our fit and the data cannot be avoided if we adopt an axisymmetric eigenfunction with respect to the pulsation axis, so it is clear that the pulsation is not exactly aligned with the tidal axis. The modeled surface amplitude distribution of the pulsation is shown in Fig. 6, again showing the higher amplitude near the tidal axis.

2.2 Spectroscopy

HD 74423 was spectroscopically followed up using the 1.9m telescope at the South African Astronomical Observatory (SAAO), Sutherland. We were able to obtain six spectra on 3 different nights (namely 24th, 25th and 27th May 2019) using the "Spectrograph Upgrade: Newly Improved Cassegrain" (SpUpNIC) spectrograph. The high resolution blue grating 4 (G4) was used in each case and the exposure time was 400 seconds to result in continuum S/N ratios between $220 - 260$ per individual exposure. The effective resolution of the spectra is 2Å. We took Copper-Argon (CuAr) lamp spectra for wavelength calibration purposes. All spectra were reduced and continuum normalized using the available Image Reduction and Analysis Facility (IRAF) routines.

The spectra were analysed with the program `SPECTRUM` (Gray & Corbally 1994)[2] and ATLAS9 model atmospheres (Castelli & Kurucz 2003). We fixed $\log g$ to 3.5. In that way we derived $T_{\rm eff} = 8000 \pm 150$ K, $[M/H] = -1.5 \pm 0.1$, and $v \sin i < 60$ kms^{-1} . This is somewhat, but not significantly different from the values derived by Gray et al. (2017). That HD 74423 is a λ Bootis star implies that its surface abundances do not reflect its interior chemical composition. The star is not overall metal-poor, as demonstrated by the presence of a number of carbon lines not reproduced by a stellar atmosphere with $[M/H] = -1.5$. We therefore confirm HD 74423 as a λ Bootis type star, and show part of the analysis in Fig. 7.

To determine the radial velocities of the star during the observations, we used a cross-correlation technique. We used

[2] http://www.appstate.edu/ grayro/spectrum/spectrum.html

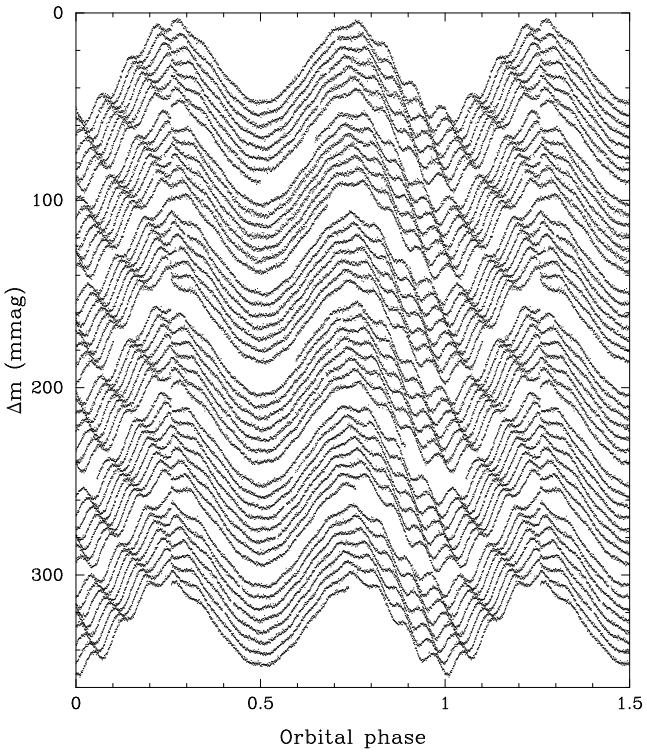

Figure 2. The orbitally stacked TESS light curve of HD 74423. Time runs from top to bottom; the light curve of each binary orbit is shifted by +6 mmag from the previous one. For clarity, one and a half orbital periods are shown. It can be clearly seen that the short-period oscillations are orbitally modulated, reaching maximum amplitude in primary minimum and minimum amplitude in secondary minimum. Furthermore, the oscillations are not phase locked with the orbital variation, which means that they are self-excited and not triggered by tidal forces.

Table 2. Radial velocity measurements of HD 74233

HJD - 2450000 d	Orbital phase	RV (barycentric) kms^{-1}
8628.2331593	0.4849	$+12.1 \pm 1.6$
8629.2450106	0.1249	$+10.8 \pm 1.2$
8631.2184967	0.3735	$+24.2 \pm 1.5$

the average spectrum of the star as a template. The absolute values of the radial velocities were calculated by cross-correlating the template spectrum with a theoretical one computed with `SPECTRUM`. We found that using the metallic-line spectrum redwards of 4200Å gave the most reliable results, which are listed in Table 2. The radial velocity measured in the last night is significantly different from the others, suggesting the presence of a companion. However, we do not yet understand the dependence on orbital phase, which should be the opposite.

2.3 Basic stellar parameters

The Gaia DR2 parallax of HD 74233 is 2.04±0.03 mas. With $V = 8.61$ and $E(B-V) = 0.055$ (Sect. 1.1), this results in $M_v = -0.02 \pm 0.04$. With the bolometric correction taken from Flower (1996) we arrive at $M_{\rm bol} = -0.05 \pm 0.04$, and with $M_{\rm bol} = 4.74$ for the Sun (Livingston 2000), we obtain $\log L = 1.92 \pm 0.02$. Assuming $T_{\rm eff} = 8050 \pm 150$ K (Sect. 1.1, 2.2) yields $R = 4.66 \pm 0.18\,\mathrm{R}_\odot$.

Figure 8 shows a comparison of these parameters with theoretical stellar evolution tracks, computed with the MESA stellar evolution code (Paxton et al. 2011) using a metallicity of $Z = 0.012$. The models include moderate overshoot and rotational mixing, and are initialized with rotational velocities of $50\,\mathrm{kms}^{-1}$ at the ZAMS. These models suggest $M = 2.33 \pm 0.03\,\mathrm{M}_\odot$, but the measurement error is likely to be far smaller than uncertainties associated with the stellar models. A different rotational velocity or metallicity would add much larger systematic contributions of a few tenths of a solar mass. The primary lies near the TAMS, though it is not clear whether it has exhausted hydrogen in its core. In any case, with the mass and radius thus determined, we confirm that $\log g = 3.47 \pm 0.04$ and derive the pulsation constant for the single variability frequency with $Q = 0.017 \pm 0.001$, which is expected for δ Scuti pulsation near the hot border of the instability strip. Given the evolutionary state of the star, this would still be a high-order mixed mode, with the major contribution to mode energy stemming from the g-mode cavity.

2.4 Modelling the ellipsoidal variations

A first model of HD 74423 was created using Phoebe 2.1 (Horvat et al. 2018). We started from the known parameters of the system (e.g. period, teff, mass, radius of the primary) and changed them until decent agreement with the light curve was achieved. The model was compared with phase folded and binned light curve by eye. The main finding of this exercise was that there is only a very small range of the mass ratio of the system that allows the primary to not overflow. The primary minimum was fairly well reproduced, while the correct depth of the secondary minimum could not be achieved. The best-fit parameters were: q = 0.076, inclination $i = 45^o$, primary mass = $2.1\,\mathrm{M}_\odot$, primary $T_{\rm eff}$ = 8300 K, primary radius = $4.4\,\mathrm{R}_\odot$, secondary $T_{\rm eff}$ = 3000 K, secondary radius = $1.0\,\mathrm{M}_\odot$. This suggests an inflated secondary star. However, since this is a "blind" best-fit result, and possible degeneracies with, e.g., the assumed gravity darkening exponent assumed, exist, we hesitate to accept this possibility.

3 TIDAL FOCUSING OF ACOUSTIC MODES

In a tidally distorted star, the usual quantities such as Brunt-Vaisälä frequency and Lamb frequency that govern pulsation dynamics are no longer spherically symmetric. The star's pulsation modes are no longer described by spherical harmonics, and the linearized oscillation equations become very complicated. Rather than solve the full problem, here we present a WKB analysis for waves in a tidally distorted star. We shall demonstrate that waves can be tidally confined or

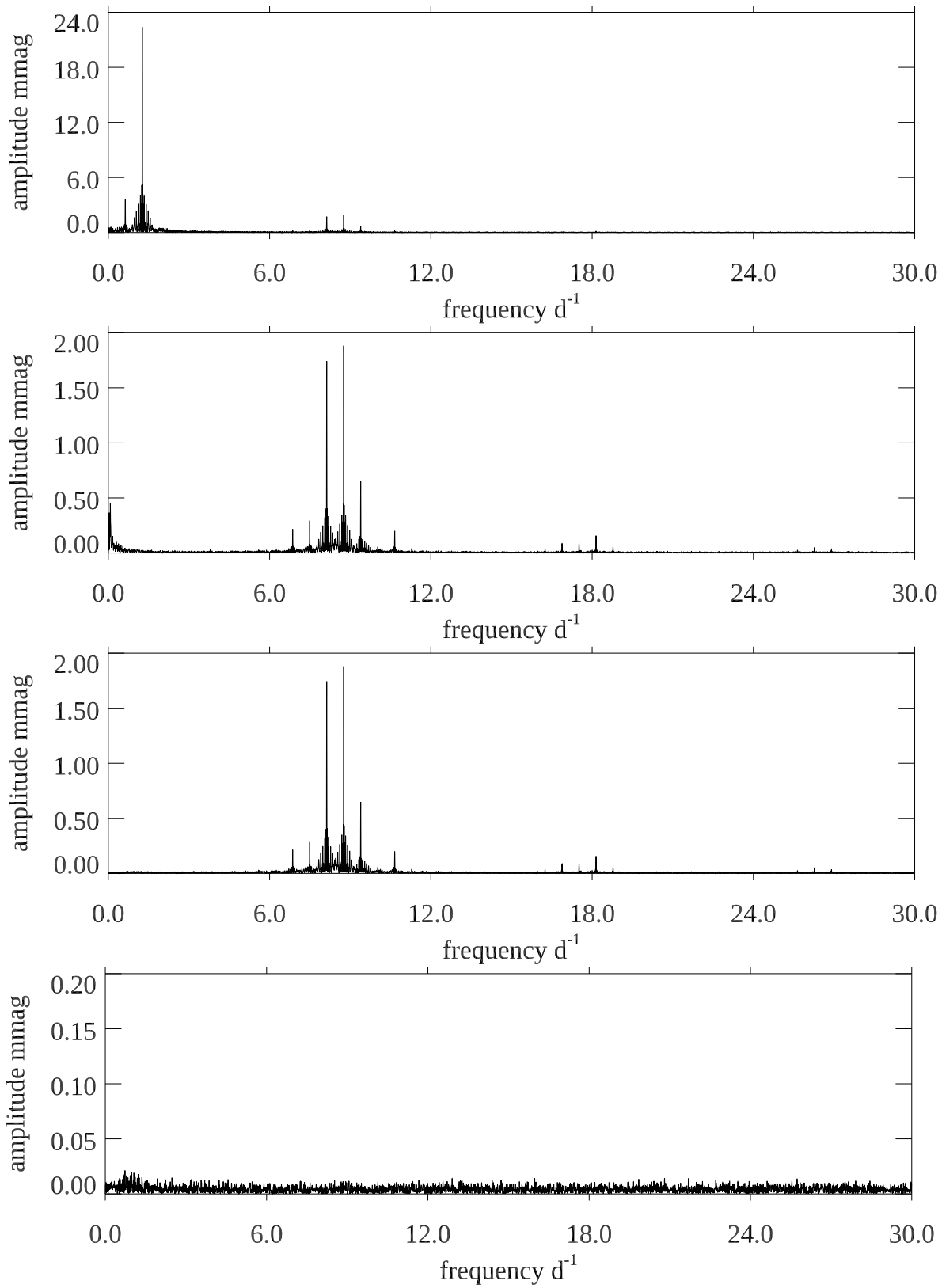

Figure 3. Top: The initial amplitude spectrum of the light curve of HD 74223, where the highest peak is at twice the orbital frequency, $\nu_{\rm orb} = 0.6326218 \pm 0.0000006\,{\rm d}^{-1}$. Second panel: The amplitude spectrum of the residuals after pre-whitening a harmonic series of five terms based on the orbital frequency. It can be seen that there are low frequency peaks, which are instrumental artefacts. The pulsation multiplet centered around $\nu_1 = 8.756917 \pm 0.000010\,{\rm d}^{-1}$ and its harmonics are visible. The third panel shows the same as the second, but after the high-pass filter has removed the low-frequency artefacts. The multiplets can easily be seen. The bottom panel shows the amplitude spectrum of the residuals after the fit shown in Table 1. Note the changes in ordinate scale.

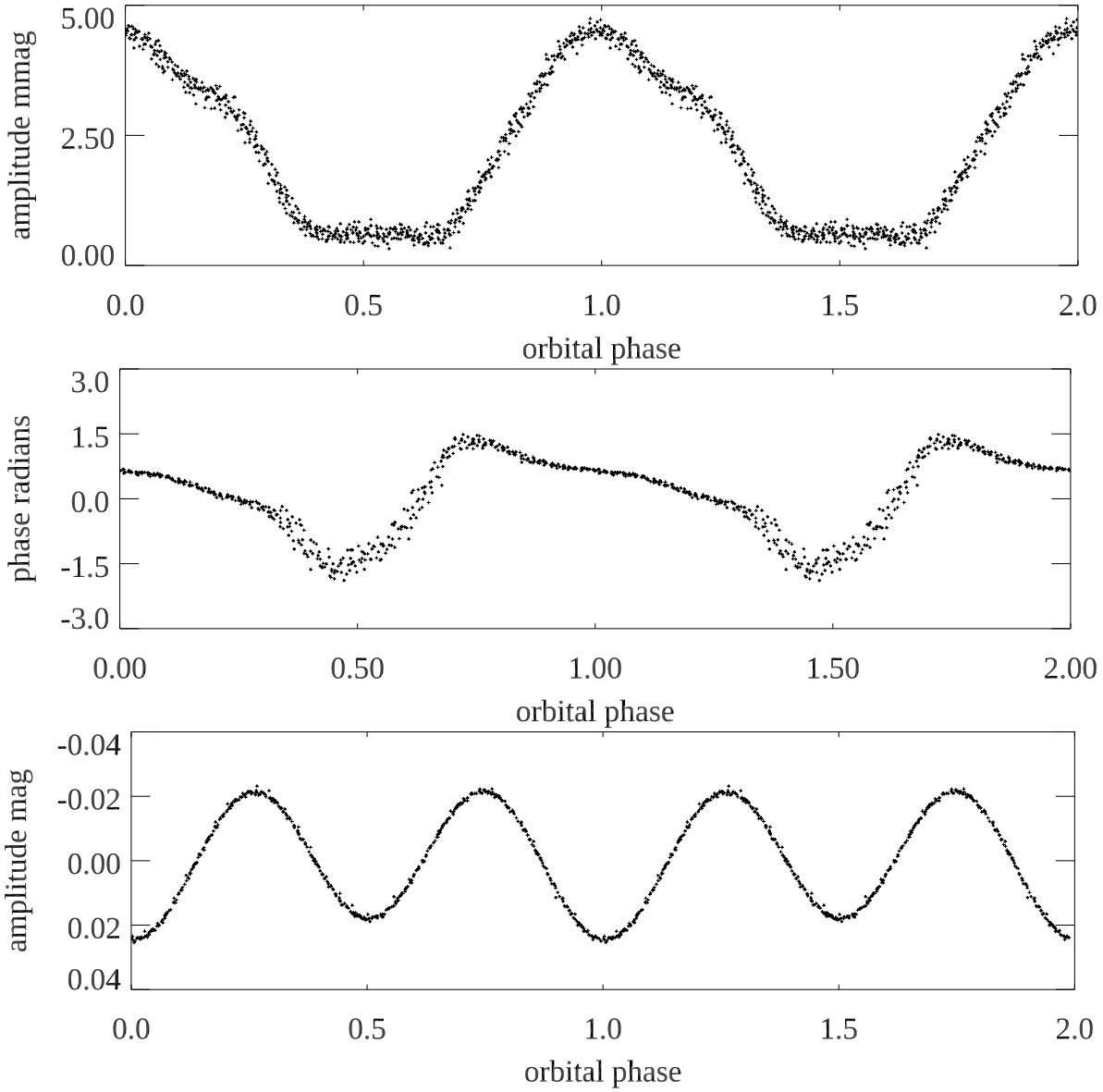

Figure 4. Top: The amplitude variation as a function of orbital phase, taking $\nu_1 = 8.756917\,\mathrm{d}^{-1}$ to be the pulsation frequency. The zero point in time is $t_0 = \mathrm{BJD}\,2458584.78684$, which was chosen to set the two first orbital sidelobes to have equal phase. That coincides with pulsation amplitude maximum, as expected for an oblique pulsator. Middle: the pulsation phase variation over the orbital cycle with a range of 2π radians. The quicker phase reversals come at amplitude minimum. Bottom: the orbital light variations as a function of orbital phase for comparison. The data have been binned to 200-s, and the pulsation variations have been removed. It can be seen that orbital light minimum coincides with pulsation maximum, as expected in the oblique pulsator model.

amplified in certain parts of the star, especially the region near the first Lagrange (L1) point. Hence, the surface flux peturbation of a pulsation mode formed by such a tidally focused standing wave would be largest near the L1 point, as we observe in HD 74423.

Below, we consider a tidally distorted star that is symmetric about the tidal distortion axis, i.e., the line of apsides. Real tidally distorted stars are not symmetric about this axis because they are centrifugally distorted via rotation. For simplicity we neglect the centrifugal distortion and Coriolis forces (as they are typically less important than tidal distortion), and consider stellar quantities to be a function of radial coordinate r and angular coordinate θ away from the tidal axis.

We begin with the WKB dispersion relation for adiabatic gravitoacoustic modes in a spherically symmetric star,

$$k_r^2 = \frac{(N^2-\omega^2)(k_\perp^2 c_s^2 - \omega^2)}{c_s^2\omega^2} - \frac{\omega_c^2}{c_s^2}\,. \tag{4}$$

Here, k_r is the radial wavenumber, ω is the wave frequency, N is the Brunt-Vaisälä frequency, c_s is the (adiabatic) sound speed, $k_\perp$ is the horizontal wavenumber, and $\omega_c = c_s/(2H)$ is the acoustic cutoff frequency, with H the density scale height.

Equation 4 is not exact, as each of the quantities (other than ω) will be a function of angular coordinate in a tidally distorted star. Nonetheless, the WKB dispersion relation

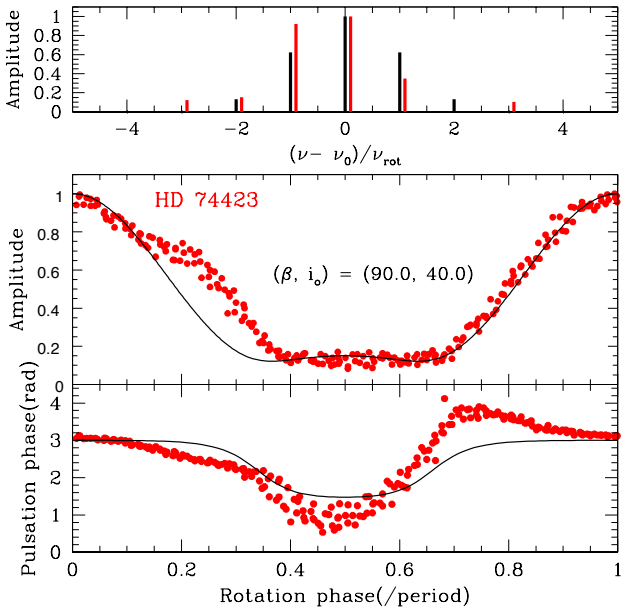

Figure 5. Top: comparison of the multiplet amplitudes (red lines) and those of our best-fit model (black lines) normalised by the amplitude of the central frequency. Middle: amplitude modulation of HD 74233 (red dots) compared with the model (black lines). Bottom: same comparison, but for the phase modulation.

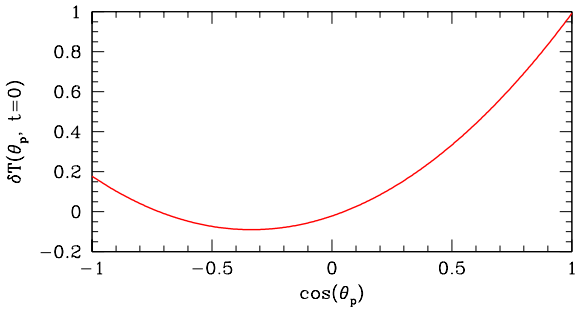

Figure 6. Temperature perturbation at the initial pulsation phase as a function of $\cos\theta_{\rm p}$. This indicates pulsation amplitude to be trapped in the hemisphere toward the companion.

is a reasonable approximation as long as the wavenumber k_r is larger than the inverse of the horizontal scale height $H_\perp \sim 1/r$, which is length scale over which quantities vary in the horizontal direction (i.e., along equipotentials). Acoustic waves propagate where $\omega > k_\perp c_s$, so we now focus on the limit $\omega \gg k_\perp c_s$, which is valid in the outer layers of the star where the sound speed is small. Then we find

$$k_r^2 \simeq \frac{\omega^2 - N^2 - \omega_c^2}{c_s^2}\,. \qquad (5)$$

This is the usual acoustic wave dispersion relation, but we have kept the N^2 term which could be important for laterally confining the waves in δ-Scuti stars with stably stratified envelopes. We can also solve for the wave frequency,

$$\omega^2 \simeq k_r^2 c_s^2 + N^2 + \omega_c^2\,. \qquad (6)$$

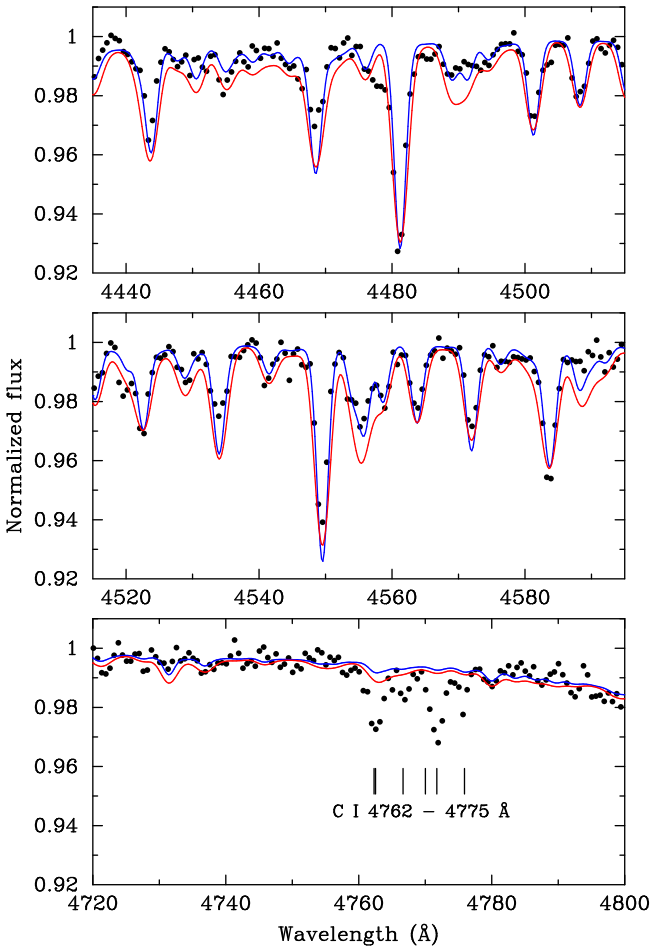

Figure 7. Selected parts of the averaged metallic-line spectrum of HD 74423 as obtained on 24 May 2019 ($S/N \approx 350$.) The observations are shown as black dots. The blue line represents a model atmosphere fit with $\log g = 3.5$, $T_{\rm eff} = 8000$ K, $[M/H] = -1.5$, and $v \sin i = 0\,{\rm km s^{-1}}$. The red line shows a model atmosphere fit with the same $\log g$ and $T_{\rm eff}$, but $[M/H] = -1.3$, and $v \sin i = 100\,{\rm km s^{-1}}$. Top two panels: rotation with $v \sin i = 100\,{\rm km s^{-1}}$ is not consistent with the observations, as it results in a poor fit of, e.g., the line blends near 4515, 4530 and 4555 Å or the single lines 4445 and 4585 Å. Lower panel: $[M/H] = -1.5$ cannot explain the strength of the CI 4762 – 4775 Å multiplet, corroborating that HD 74423 has abundance anomalies of the λ Bootis type.

The wave turning points in the radial direction can be calculated by determining where the radial group velocity is equal to zero,

$$\begin{aligned}\frac{\partial\omega}{\partial k_r} &= 0\\ &= \frac{k_r c_s^2}{k_r^2 c_s^2 + N^2 + \omega_c^2}\\ &= \frac{c_s(\omega^2 - \omega_c^2 - N^2)}{k_r^2 c_s^2 + N^2 + \omega_c^2}\,. \end{aligned} \qquad (7)$$

So we see the turning point in the radial direction occurs where

$$\omega^2 = N^2 + \omega_c^2\,. \qquad (8)$$

which is the usual condition for the outer turning point.

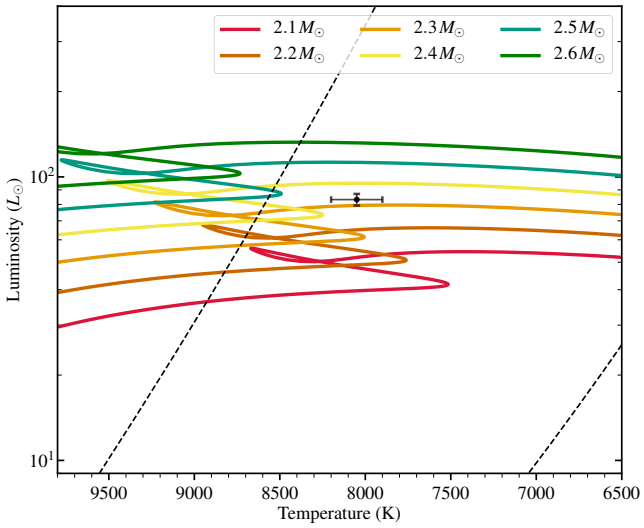

Figure 8. The position of HD 74423 (full circle with error bar) in a theoretical HR diagram. Model evolutionary tracks (full lines) are labeled with their masses. The boundaries of the δ-Scuti instability strip (Murphy et al. 2019) are shown with dotted lines.

Now let us examine the horizontal domain of wave propagation, recalling that N^2 is a function of angular coordinate θ away from the tidal axis. Solving equation 4 for the wave frequency,

$$\omega^4 - (k^2c_s^2 - N^2 - \omega_c^2)\omega^2 + k_\perp^2 c_s^2 N^2 = 0\,. \tag{9}$$

Solving for ω^2 in the limit that the $k_\perp$ term is small, we find

$$\omega^2 \simeq k^2c_s^2 + N^2 + \omega_c^2 - \frac{k_\perp^2 c_s^2 N^2}{k^2c_s^2 + N^2 + \omega_c^2}\,. \tag{10}$$

The horizontal turning point of the wave occurs where

$$\begin{aligned}\frac{\partial\omega}{\partial k_\perp} &= 0 \\ &\rightarrow 2k_\perp c_s^2 - 2k_\perp \frac{c_s^2 N^2}{k^2c_s^2 + N^2 + \omega_c^2} \simeq 0 \\ &\rightarrow k^2c_s^2 \simeq -\omega_c^2\,.\end{aligned} \tag{11}$$

Using the dispsersion relation from equation 5, we find the horizontal turning point occurs where

$$\omega^2 \simeq N^2\,. \tag{12}$$

So, in a tidally distorted star where N^2 is smaller near the tidal distortion axis, there may exist waves which locally have $\omega^2 > N^2$ and hence propagate near the tidal axis. Away from the tidal axis where N^2 increases, the waves will encounter a turning point, and will hence be confined to latitudinal coordinates near the tidal axis. This angular trapping can only occur for waves with frequencies in the range

$$N^2(\theta = 0) < \omega^2 < N^2_{\rm max}\,, \tag{13}$$

where $N^2_{\rm max}$ is the maximum value of N^2 at any latitudinal coordinate away from the tidal axis. In a spherical star, N^2 is the same at all latitudinal coordinates, and hence latitudinally trapped waves do not exist.

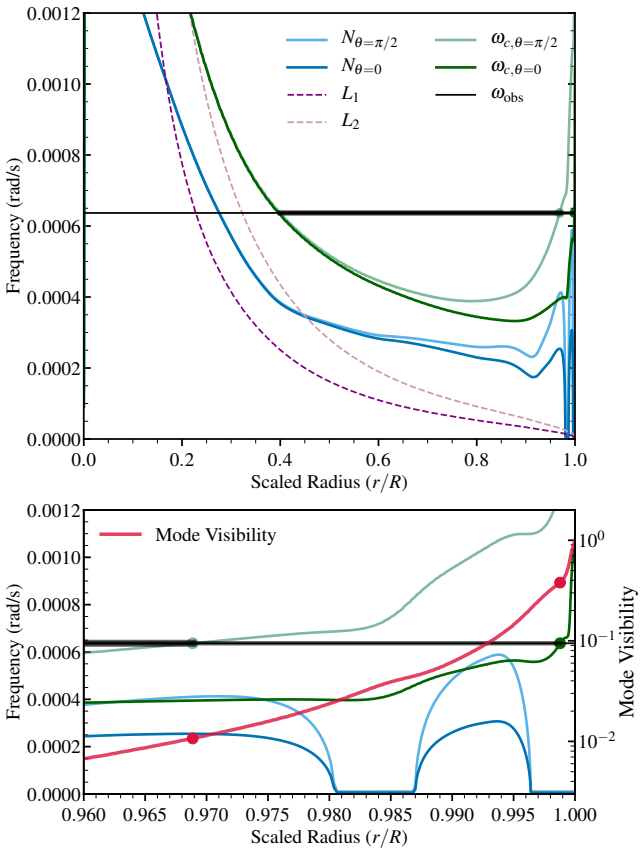

Figure 9. Top: Propagation diagram illustrating how acoustic modes can be tidally amplified near the tidal axis. The dark and light blue lines show the Brunt-Vaisälä frequency near and far from the tidal axis, and similarly the dark and light green lines show the acoustic cutoff frequencies. The dashed lines show $\ell = 1$ and $\ell = 2$ Lamb frequencies, which are irrelevant for tidally focused p modes. The black line shows the observed mode frequency in HD 74423, with thick lines indicating the acoustic mode cavity at different tidal latitudes. **Bottom:** A zoom-in on the surface layers. Tidal amplification occurs because acoustic waves can propagate much closer to the stellar surface near the L1 point compared to other latitudes, producing much larger flux perturbations (red line).

Figure 9 shows a propagation diagram for a 2.3 $M_\odot$ stellar model from MESA (Paxton et al. 2011) that matches the surface temperature and radius of HD 74423. We have plotted approximations of the Brunt-Vaisälä and acoustic cutoff frequencies, N and ω_c, at a latitude near the tidal axis and the tidal equator. In principle, tidal confinement could occur for a wave with frequency between the two values of N, though the observed pulsation in HD 74423 has too high frequency to be latitudinally tidally confined. Additionally, because we find $\omega_c > N$ for this star, tidally confined acoustic waves would be evanescent. Hence, tidal confinement as discussed above is unlikely to be occurring in this system.

Instead, we are likely seeing a mode amplification effect caused by the tidally distorted structure of the star. Because the acoustic cutoff frequency ω_c varies with latitude, so does the outer turning point of acoustic waves. The bottom panel shows that a wave at the pulsation frequency

in HD 74423 has an outer turning point $r/R \simeq 0.97$ near the tidal equator, but has a turning point $r/R \simeq 0.998$ near the L1 point. Because the density and sound speed drop sharply near the surface, the amplitude of a propagating acoustic wave increases, with the radial displacement scaling as $\xi_r \propto (\rho r^2 c_s)^{-1/2}$ in the WKB limit. The surface flux perturbation of a mode scales as $\delta F/F \propto \delta T/T$, which approximately scales as $\delta T/T \sim k_r \xi_r$. So, even if pulsation energy is independent of latitude, we expect the mode visibility to scale approximately as $\delta F/F \propto k_r \xi_r \propto (\rho r^2 c_s^3)^{-1/2}$ at the outer turning point of the wave. Figure 9 demonstrates this quantity is larger by more than an order of magnitude at the tidal axis for the observed pulsation frequency, hence the pulsation amplitude is greatly tidally amplified near the L1 point. This can largely explain the amplitude modulation of the pulsation in HD 74423, including the fact that the amplitude is smaller (but still non-zero) at orbital phases when the L1 area is hidden from view.

We note the tidal amplification effect is much more pronounced for low frequency modes. Figure 9 shows that a mode of twice the frequency would have its outer turning point much closer to the surface near the tidal equator, so that the relative tidal amplification near the L1 point is much smaller. HD 74423 pulsates in a very low order (likely $n = 1$) p mode, so the tidal amplification effect is more pronounced compared to typical δ-Scutis pulsating in higher overtones. Additionally, HD 74423 has only one detectable pulsation mode, simplifying its power spectrum and facilitating the identification of the mode's amplitude modulation. These effects help explain why HD 74423 is the first star in which tidal trapping has been recognized, but they suggest many other pulsators in close binaries may also exhibit signs of tidal trapping.

4 POLYTROPE-ROCHE MODELLING

We saw above that angular variations in the acoustic cutoff frequency ω_c can produce angular variations in a pulsation mode's surface flux perturbations. In order to get a sense for the range of acoustic cutoff frequencies within the tidally disorted primary of HD 74423, we utilize a polytropic approximation to mdoel the stellar interior. The effective potential in a frame rotating with the binary orbit can be written as:

$$\Psi_{\rm eff} = \Psi_1 + \Psi_2 + \Psi_{\rm cent} \tag{14}$$

where the three terms are the potential of star 1, the potential of star 2 (taken to be a point mass), and the fictitious centrifugal potential, respectively. The equation of hydrostatic equilibrium in the rotating frame can be expressed as:

$$\frac{1}{\rho}\vec{\nabla}P = \vec{g}_{\rm eff} = -\vec{\nabla}\Psi_{\rm eff} \tag{15}$$

For a polytropic gas, $P = K\rho^{1+1/n}$, where n is the polytropic index, which is related to the ratio of the heat capacities, $C_p/C_v \equiv \gamma = 1 + 1/n$, and K is the constant of proportionality. The left-hand side of Eqn. (15) can be written for the case of a polytrope as

$$\frac{1}{\rho}\vec{\nabla}P = K(n+1)\vec{\nabla}\rho^{1/n} \tag{16}$$

In that case we can rewrite the equation of hydrostatic equilibrium as:

$$\vec{\nabla}\left[K(n+1)\rho^{1/n} + \Psi_{\rm eff}\right] = 0 \tag{17}$$

where the solution is

$$K(n+1)\rho^{1/n} + \Psi_{\rm eff} = \Psi_{\rm eff,0} \tag{18}$$

and $\Psi_{\rm eff,0}$ is the effective potential where the density, ρ goes to zero. Finally, we can write an analytic expression for the density everywhere within star 1 as long as the effective potential is known:

$$\rho = \left[\frac{\Psi_{\rm eff,0} - \Psi_{\rm eff}}{K(n+1)}\right]^n \tag{19}$$

In the case of a Roche-lobe filling star, $\Psi_{\rm eff,0} = \Psi_{\rm RL}$, where $\Psi_{\rm RL}$ is the potential at the Roche surface.

In order to solve for the density in Eqn. (19) we need only approximate the potential of star 1 (Ψ_1) since Ψ_2 and $\Psi_{\rm cent}$ are already known. Deep in the interior of star 1, the star is essentially spherically symmetric and largely unaffected by Ψ_2 and $\Psi_{\rm cent}$. Thus we start the interior of star 1 by building a polytropic model. Near where the surface of the unperturbed polytrope would be (and, in fact, well below its surface), the potential goes approximately as $\propto 1/r$ since most of the mass is concentrated near the center.

The procedure we use is to construct a polytrope for the unperturbed problem with a radius that fits completely inside the equivalent Roche surface. To this end, we define four distances from the center of star 1 to the unperturbed Roche potential, $R_{\rm x1}$, $R_{\rm x2}$, $R_{\rm y}$, $R_{\rm z}$. These are along the x, y, and z directions, as implied by the name, and the subscripts '1' and '2' refer to the direction toward the L1 point and away from it, respectively. We then set the nominal radius of the polytropic model to be $R_{\rm z}$, which is the smallest of the four distances. Since HD 74423 is fairly massive ($M_1 \simeq 2.4\,M_\odot$) and hot ($T_{\rm eff} \simeq 8000$ K), we model it as an $n = 3$ polytrope, which does not yield an accurate density profile near the center (since the star is somewhat evolved), but should be quite adequate further out where we care most about the run of density and temperature. Thus, from hereon out, the discussion is not general for all polytropes and is limited to $n = 3$ polytropes.

The values of the polytropic constants for the problem, in terms of the mass, M_1, and radius, R_1 of the star are:

$$K = \pi G\left[\frac{M_1}{-4\pi\xi_1^2(d\phi/d\xi)_1}\right]^{2/3} \tag{20}$$

$$\rho_{\rm c} = -\frac{\xi_1 M_1}{4\pi R^3 (d\phi/d\xi)_1} \tag{21}$$

$$a = \sqrt{\frac{K}{\pi G}}\,\rho_{\rm c}^{-1/3} \tag{22}$$

where ρ_c is the central density, a the length scale, ϕ the Lane-Emden solution for an $n = 3$ polytrope, ξ the dimensionless radial distance, ξ_1 is ξ evaluated at the unperturbed surface of the polytrope, and $(d\phi/d\xi)_1$ is the derivative of the Lane-Emden function at the surface. The density, temperature, and potential (Ψ_1) inside the star are:

$$\rho(\xi) = \rho_{\rm c}\phi(\xi)^n \tag{23}$$

$$T(\xi) = \frac{\mu K}{k}\rho_{\rm c}^{1/n}\phi(\xi) \tag{24}$$

$$\Psi_1(\xi) = -\frac{GM_1}{R_1} - 4K\rho_{\rm c}^{1/3}\phi(\xi) \tag{25}$$

where k is Boltzmann's constant, and the radial distance $r \equiv a\xi$.

In order to make the model completely analytic, we utilize an approximation to the solution for the Lane-Emden equation for an $n = 3$ polytrope:

$$\phi(\xi) \simeq \frac{1 - (1/108)\xi^2 - (11/45360)\xi^4}{1 + (17/108)\xi^2 + (1/1008)\xi^4} \tag{26}$$

where $\phi \to 0$ when $\xi = 6.89685$ for an $n = 3$ polytrope. This expression and its derivative (needed to compute the local gravity) are good to ∼1%, which is quite adequate for our purposes.

Thus, in Eq. (19) we use $\Psi_1(\xi)$ from Eqn. (25) for $r = a\xi \lesssim R_z$, and $\Psi_1(r) = -GM_1/r$ for $r \gtrsim R_z$. In fact, we use a hyperbolic tangent blending function between the two forms for Ψ_1 over a blending range of ∼10% of R_z to ensure a smooth transition. The density inside the Roche lobe is then everywhere determined analytically by the use of Eqn. (19). The pressure, temperature, and local sound speed follow from the polytropic relations, and $\vec{g}_{\rm eff}$ is found from Eqn. (15).

Finally, in regard to the binary model, we note that the mass within the Roche lobe, but beyond a radial distance of R_z, contributes less than ∼0.1% of the total mass M_1. Therefore, the basic relation among the orbital period, M_1, M_2, and semimajor axis (i.e., Kepler's 3rd law), is not materially affected beyond the fractional percent level (see detailed calculations by .. reference).

As discussed in Section 3 we take the acoustic cutoff frequency as

$$\omega_c \simeq \frac{c_s}{2H} \simeq \frac{(1 + 1/n)g}{2c_s}\,. \tag{27}$$

where c_s is the local sound speed $c_s = \sqrt{\gamma P/\rho}$. The second equality in equation 27 stems from the relation $H = c_s^2/[(1+1/n)g]$ for polytropes. Hence, it is instructive to examine the tidally perturbed acoustic cutoff frequency for a $n = 3$ polytrope,

$$\omega_{\rm crit} \simeq \frac{2g_{\rm eff}}{3c_s}\,. \tag{28}$$

In Fig. 10 we show $\omega_{\rm crit}$ in the orbital plane of the binary. The color scale is set to emphasize the lowest values of $\omega_{\rm crit}$, which appear in the tidal bulge near the L1 point. In Fig. 11 we show a more quantitative plot of $\omega_{\rm crit}$ along the line joining the two stars, and extending from $-R_{x2}$ to $+R_{x1}$, the latter corresponding to the inner Lagrange point. Finally, in Fig. 12 we show plots of $\omega_{\rm crit}$ as a function of tidal latitude θ in the equatorial plane, for four different radial distances. Note that in all three figures, one can see that in the tidal bulge region, $\omega_{\rm crit}$ is ∼20% lower than anywhere else around the stellar longitude at comparable distances from the center.

Figures 11 and 12 demonstrate how low overtone acoustic modes are tidally amplified near the L1 point. Near the L1 point, the pulsation frequency is larger than the acoustic cutoff frequency all the way to the stellar surface, allowing acoustic modes to propagate close to the photosphere and create large flux perturbations. At other latitudes, $\omega < \omega_c$ well below the photosphere, creating smaller flux perturbations. Future work should examine this tidal amplification effect to predict the flux perturbation across the surface of the star.

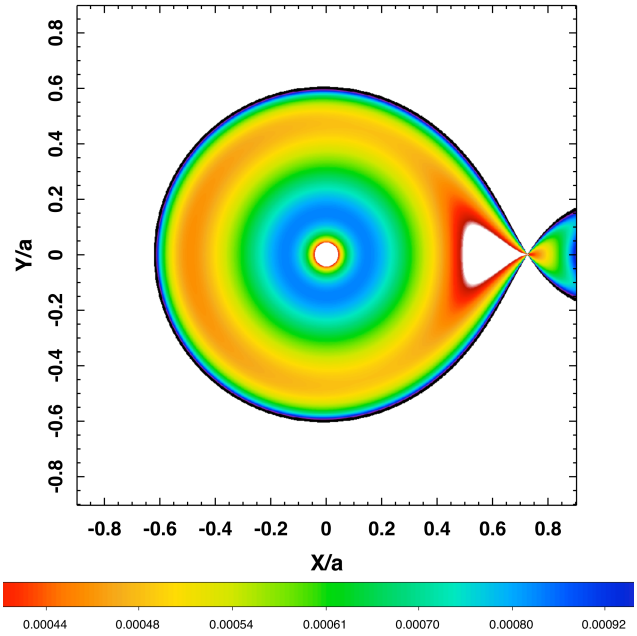

Figure 10. Acoustic cutoff frequency $\omega_{\rm crit}$ in the plane of the binary. The color coding is set to emphasize the lower values of $\omega_{\rm crit}$ in the vicinity of the inner Lagrange point.

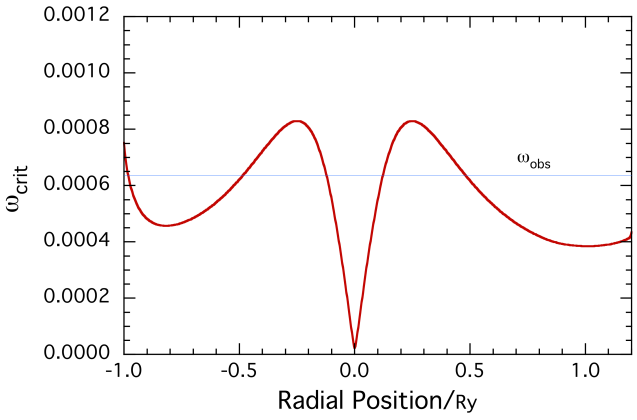

Figure 11. Acousti cutoff frequency $\omega_{\rm crit}$ plotted along the line connecting the two stars.

5 CONCLUSIONS

We report the discovery of oblique pulsation in the A star HD 74423 (TIC 355151781), aligned with tidal bulge created by its binary companion. This star shows a single pulsation mode that generates a frequency multiplet split by the orbital frequency, and the frequency/phase pattern demonstrate that the pulsation axis is the line apsides. HD 74423 is the first obliquely pulsating star known where the pulsation axis is defined by the tidal distortion. Furthermore, and most interestingly, we show in this work that the star is effectively only pulsating in the hemisphere facing its companion. We have shown that acoustic modes can propagate closer to the stellar photosphere near the L1 point, produc-

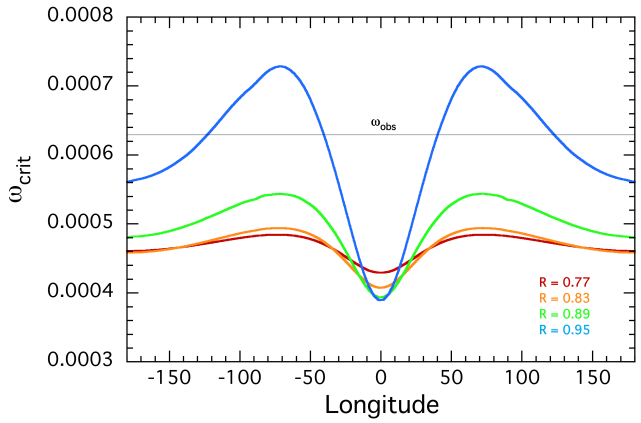

Figure 12. Acoustic cutoff frequency $\omega_{\rm crit}$ in the orbital plane, plotted as a function of the longitude at four different radial distances from the center of the star 1. The radial distances are normalized in units of R_y. Deep in the star, the observed mode propagates at all longitudes, but near the surface it only propagates near the L1 point ($\theta = 0$), producing a larger flux perturbation on that side of the star.

ing much larger flux perturbations on that side of the star, qualitatively consistent with our observations.

The pulsation mode is HD 74423 is currently unique, but there must be a class of such stars, and this discovery is an impetus to search for more. It also motivates more detailed studies of the interaction between stellar pulsations and tidal distortion in binary stars. We know from the heartbeat stars that tides do excite modes that are nearly resonant with orbital harmonics. Although we do not have a statistical study yet, our own examination of *Kepler* and *TESS* data suggests that many close binary stars in the lower instability strip do not pulsate, yet some do. Do tides in binary stars impact the excitation of p modes and g modes? While the answer to this question remains unclear, HD 74423 and other stars like it (when they are found) may reveal the solution.

ACKNOWLEDGEMENTS

This paper includes data collected by the *TESS* mission. Funding for the *TESS* mission is provided by the NASA Explorer Program. Funding for the *TESS* Asteroseismic Science Operations Centre is provided by the Danish National Research Foundation (Grant agreement no.: DNRF106), ESA PRODEX (PEA 4000119301) and Stellar Astrophysics Centre (SAC) at Aarhus University. We thank the *TESS* team and staff and TASC/TASOC for their support of the present work. GH, SC and PS acknowledge financial support by the Polish NCN grant 2015/18/A/ST9/00578. SC is grateful to Chris Engelbrecht for introducing him to the use of the observing equipment. GH thanks Ernst Paunzen for helpful discussions on the spectra of λ Bootis stars.

REFERENCES

Aerts, C., Christensen-Dalsgaard, J., & Kurtz, D. W., 2010, Asterseismology, (Springer-Verlag, Berlin)
Asplund M., Grevesse N., Sauval A. J., Allende Prieto C., Kiselman D., 2004, A&A 417, 751
Balona, L. A., 1985 MNRAS 217, 17p
Bernhard, K., Hümmerich, S., Otero, S., Paunzen, E., 2015, A&A 581, 138
Bigot, L., Kurtz, D. W., 2011, A&A 536, A73
Bohlender D. A., Landstreet J. D., 1990, MNRAS, 247, 606
Castelli, F., Kurucz, R. L. 2003, in IAU Symp. 210, Modelling of Stellar Atmospheres, ed. N. E. Piskunov, W. W. Weiss, & D. F. Gray (San Francisco, CA: ASP), A20
Cowling, T. G., 1941, MNRAS 101, 367
Flower, P. J., 1996, ApJ, 469, 355
Fuller, J. 2017, MNRAS, 472, 1538
Gray, R. O., Corbally, C. J., 1994, AJ, 107, 742
Gray R. O., Riggs Q. S., Koen C., Murphy S. J., Newsome I. M., Corbally C. J., Cheng K.-P., Neff J. E., 2017, AJ 154, 31
Hambleton, K. M., et al., 2013, MNRAS 434, 925
Hambleton, K. M., et al., 2018, MNRAS 473, 5165
Handler, G., et al., 2002, MNRAS 333, 262
Holdsworth, D. L. Kurtz, D. W., Smalley, B., Saio, H., Handler, G., Murphy, S. J., Lehmann, H., 2016, MNRAS 462, 876
Horvat, M., Conroy, K. E., Pablo, H., Hambleton, K. M., Kochoska, A., Giammarco, J., Prša, A.,
Houk, N., Cowley, A. P., 1975, *Michigan Spectral Catalogue*, Vol. 1
Kurtz, D. W., 1982, MNRAS 200, 807
Kurtz, D. W., 1985, MNRAS 213, 773
Ledoux, P., 1951, ApJ 114, 373
Livingston, W. C., 2000, in *Allen's Astrophysical Quantities*, 4th edition, ed. A. N. Cox, Springer Verlag, p. 341
Morris, S. L., 1985, ApJ, 295, 143
Murphy, S. J., Hey, D., van Reeth, T., Bedding, T., 2019, MNRAS 485, 2380
Pamyatnykh A. A., Dziembowski W. A., Handler G., Pikall H., 1998, A&A 333, 141
Paxton, B., Bildsten, L., Dotter, A., et al. 2011, ApJS, 192, 3
Pojmański, G. 2002, Acta Astron., 52, 397
Saio, H., & Gautschy, A. 2004, MNRAS, 350, 485
Shibahashi, H., & Kurtz, D. W. 2012, MNRAS, 422, 738
Springer, O. M., & Shaviv, N. J. 2013, MNRAS, 434, 1869
Thompson, S. E., et al., 2012, ApJ 753, 86
Torres, G., Andersen, J., Giménez, A., 2010, A&ARv 18, 67
Unno, W., Osaki, Y., Ando, H., et al. 1989, Nonradial oscillations of stars
Venn, K. A., Lambert, D. L., 1990, ApJ 363, 234
Welsh, W. F., et al., 2011, ApJ 197, 4

This paper has been typeset from a TEX/LATEX file prepared by the author.